SAND-79-0385
UNLIMITED DISTRIBUTION

MASTER

STUDIES OF PARTICLE BEAM OVERLAP AND ELECTRON DEPOSITION IN THIN FOILS (U)

J. A. Halbleib and T. P. Wright

Sandia Laboratories

SF 2900 Q(7-73)

SAND-79-0385

STUDIES OF PARTICLE BEAM OVERLAP AND ELECTRON DEPOSITION IN THIN FOILS

J. A. Halbleib
Theoretical Division - 4231

and

T. P. Wright
Plasma Theory Division - 4241

Sandia Laboratories
Albuquerque, New Mexico 87185

March 1979

ABSTRACT

This report summarizes a somewhat diverse set of theoretical studies carried out in 1978 which were aimed at increasing our understanding of the physics of multiple-beam overlap and enhanced deposition in thin foils. The studies reported here involve electron and ion beam overlap in single and multiple cylindrical disks of channels, and single and multiple electron-beam deposition in thin foils. Some of the important consequences of these studies which affect ongoing research are the scaling formula derived for overlap current density gain in cylindrical geometry, an understanding of the importance of electron drift motion in thin-foil-enhanced deposition, and the necessity of providing non-axial return current paths and magnetic isolation of disks in multiple-disk configurations.

Table of Contents

List of Figures

SAND-79-0385

STUDIES OF PARTICLE BEAM OVERLAP AND ELECTRON DEPOSITION IN THIN FOILS

J. A. Halbleib and T. P. Wright
Sandia Laboratories, Albuquerque, New Mexico 87185

March 1979

I. Introduction

This report is a summary of several theoretical studies carried out in 1978 concerning multiple-beam concentration and deposition for inertial confinement fusion (ICF) applications. Since it seems unlikely that single particle-beam sources can produce the power density and energy needed to drive present ICF breakeven pellet designs, the total power required must be accumulated by overlapping multiple beams generated synchronously from several sources. The calculations reported here constitute the first attempt to identify the important physical processes which determine the overlap gain and deposition in thin targets.

Section II covers the first set of studies which addresses the amount of overlap current density gain that should be obtainable in 6 or 12 channels carrying electron or proton beams in a single cylindrical disk. The principal tool used in this study was a collisionless 3-D single-particle trajectory code which follows charged particles (electrons or ions) in prescribed fields. A simple analytical formula is given for estimating the overlap gain in single disk systems. Also, to gain insight into new physics involved with multi-disk systems, results from calculations for a 90-channel, 5-disk electron beam system are discussed.

In Section III, thin-foil deposition by electrons in several configurations using channel magnetic fields is investigated. These calculations were performed with the Monte Carlo electron-photon transport code CYLEM[1] which not only follows 3-D electron trajectories in prescribed fields, but also computes electron scattering and deposition in materials with cylindrical boundaries.

ICF net-energy-gain particle-beam-target designs seem to require[2] deposition levels 10^{13}-10^{14} W/cm^2. The requirement for thin shells comes to about 1000 TW/gm, and for thick-shell ablative pusher targets, the deposition required is about 100 TW/gm at the target outer surface. The goal of the work reported here is not to optimize a configuration to approach these deposition levels but to gain an understanding of the relevant physics involving overlap and enhanced deposition.

The knowledge gained from these studies is instrumental in the design of future multi-beam configurations which are optimized for overlap gain and deposition enhancement. There is not a strong correlation between Secs. II and III since most of the original calculations by the authors were performed independently. In the process of incorporating the multi-channel fields into the deposition code, the need to coordinate ongoing research became apparent and is now being pursued.

Section IV summarizes the knowledge gained from these studies and singles out some promising concepts which are presently under investigation.

II. Collisionless Overlap Studies

The first multi-channel overlap calculations were performed for 40 and 36 electron beams in a wagonwheel disk arrangement.[3] Since the injected beam current per channel exceeds the Alfvén-Lawson critical current for electrons (I_A), the channel must contain a highly conducting plasma to cancel the beam current.[4] The injected beam particles are contained in the channel through the application of a plasma current over a timescale much longer than the beam pulse time. The net magnetic field is obtained from superposition of the individual channel magnetic fields.[3]

The first part of the work reported here is concerned with channel configurations and electron or ion beams relevant to the Proto-II accelerator. The basic wagonwheel configuration in this case has 12 channel "spokes." Two discharge return-current configurations will be discussed. The first consists of two axial channels perpendicular to and fed by the 12 beam channels in the standard wagonwheel configuration.

The second configuration alternates beam and return channels, so that there are 6 beam channels and 6 plasma discharge return current channels in the same plane. The first configuration leads to larger net magnetic fields as the current flowing in the axial channels strengthens the superimposed beam channel fields. The net magnetic field at the edges of the channels is a minimum in the plane of the disk for the standard configuration, whereas for the alternating configuration, the net field between channels in the plane of the disk is a maximum. Thus, for the standard configuration the individual beams merge to a disk beam at the overlap radius. The alternating configuration keeps the beams from mixing azimuthally while allowing them to spread axially.

The first cases presented will be electron and ion beams injected into the standard wagonwheel configuration. Figure 1 shows the minimum radius achieved by several trajectories of 1.5-MeV electrons for two cases where the individual channel radii (r_c) were 5 mm and 3 mm, respectively. The wagonwheel axis lies along the z direction. The initial coordinate positions in a channel are shown above the plots. These were chosen to suitably cover the initial phase-space distribution of a complete set of initial points[3] and contain some worst-case trajectories. It was found that the overlap results are fairly insensitive to the details of the initial phase space distribution because of phase-mixing as the electrons propagate down the channels. As can be seen from Fig. 1, the mean value of the minimum spherical radius (R_m) is about one-fourth of the value of the cylindrical overlap radius (R_o) in both cases. The resulting current density at R_m is a factor of 3 above that in a

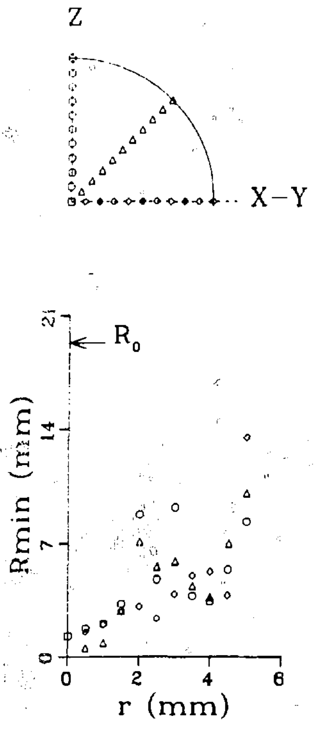

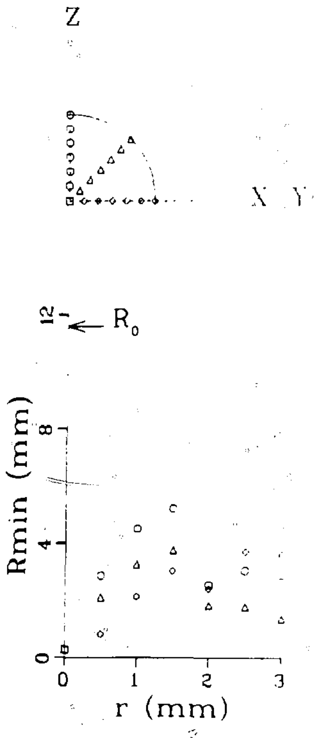

FIGURE 1

single channel. These are similar to previous results[3] and provide further evidence that the overlap results for electrons with channel currents near the Alfvén current are relatively insensitive to geometrical considerations such as the number or size of channels. We will discuss the conditions under which this is true later. We note that 12 channels are an optimum of sorts for a single disk since $R_o \approx 4\ r_c$ and $R_o \approx 4\ R_m$ so that $R_m \approx r_c$, and most of the electrons reach a minimum radius equal to the channel radius.

Next, a series of 2.0-MeV proton calculations were performed for the same configuration. The trajectory code at this point had been modified to run several histories sequentially, choosing initial phase space coordinates randomly from an isotropic or cosine distribution. Higher overlap current density gains should be achievable with ions instead of electrons since their larger mass results in less bending in the channel fields, leading to colder beams which spread more slowly after exiting a channel. Since the channel magnetic field can be chosen to preserve the initial beam half-angle spread θ_m (with respect to the channel axis), this angle is expected to play an important role in the degree of overlap attainable. To establish the relative importance of the guide magnetic field and θ_m, they were varied independently. First, two sets of ion trajectories were run with $\theta_m = 16^\circ$ in 1.5-cm diameter channels carrying currents of 50 kA and 100 kA, respectively. At 50 kA, the overlap current density gain was 4.3 and it only increased 5% for 100 kA. The results of varying θ_m with channel currents of 100 kA are shown in Fig. 2. The current density gain saturates between values

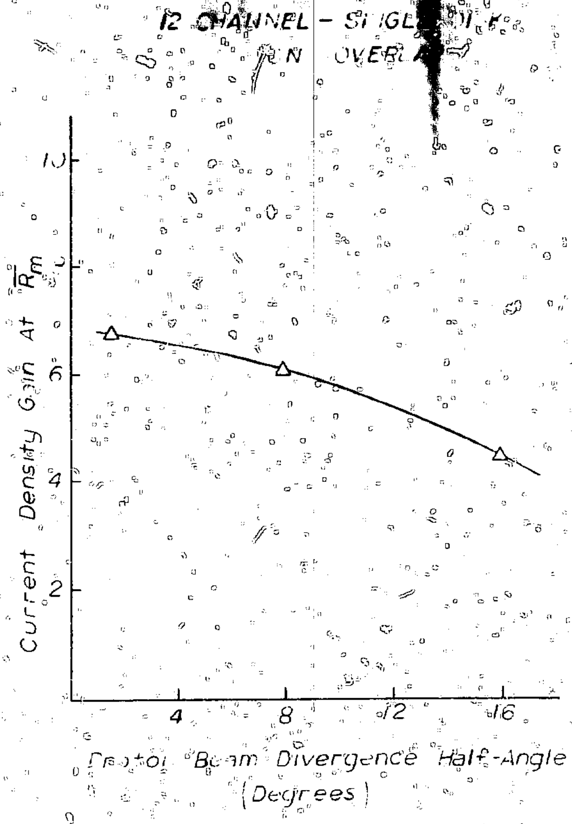

12 CHANNEL
Current Density Gain At $\overline{R}_m$
2
4
6
4
8
12
16
Beam Divergence Half-Angle
(Degrees)

FIGURE 2

of 6 and 7 for small angles. This saturation depends on the number of channels and r_m in a manner discussed below where analytical overlap estimates are given.

The alternating channel configuration arose as a suggestion during some discussions on channel configurations. Figures 3 and 4 show the difference in several r-z trajectories of electrons in the standard wagonwheel configuration and in the alternating configuration, respectively. The code has been modified to include the channel edge effect discussed in Sec. 3.3 for these calculations. Without the fields due to the axial return currents, the electrons in the alternating configuration (Fig. 4) make essentially force-free transits of the central overlap region and escape radially or axially after a single pass. Half of the plasma channels provide good transport of the electrons away from the overlap region. Figure 5 shows a comparison of the distributions of minimum spherical distance from the center of the system for the two configurations. The result for the alternating configuration is noticeably broader, principally because of the axial spreading of the beams. Since only half of the channels are being used to transport beams, the overlap current density gain drops to 1.5 from the value of 3.4 for the standard configuration. Similar results were found for protons with an 8° divergence half-angle: the current density gain dropped from 6.1 to 2.8 in the alternating configuration. Further studies of the alternating configuration were not undertaken.

Based on the trajectory calculations, it is possible to develop analytical current density gain estimates for electrons and ions. The formula[3] for the current density gain achievable from a single

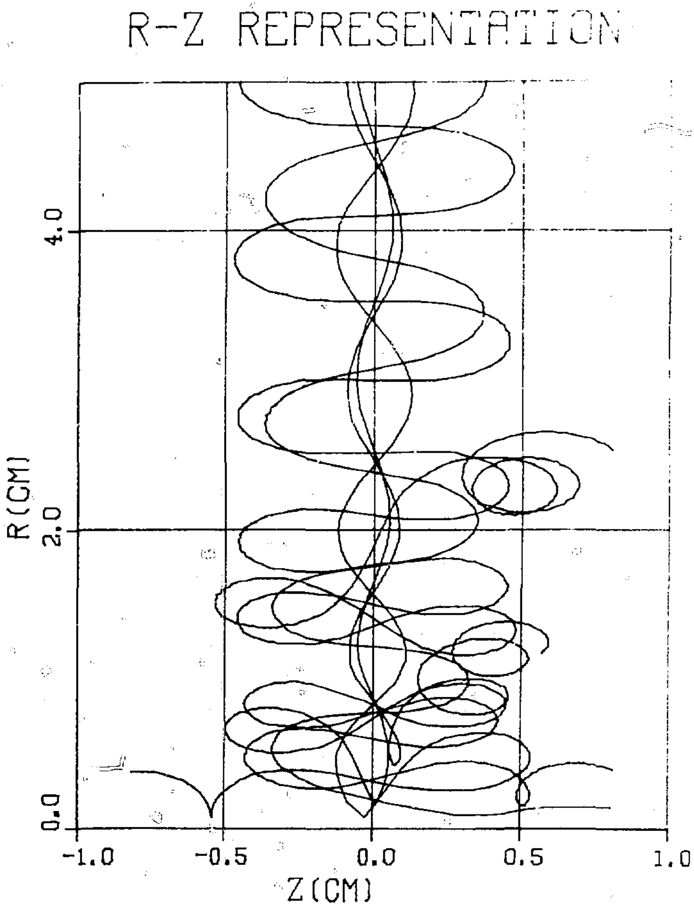

FIGURE 3

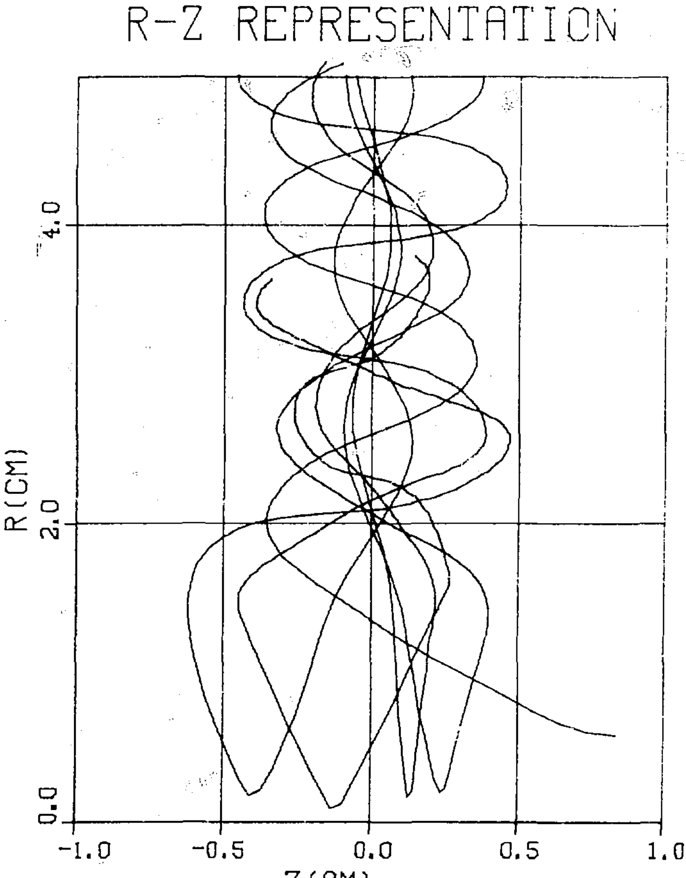

FIGURE 4

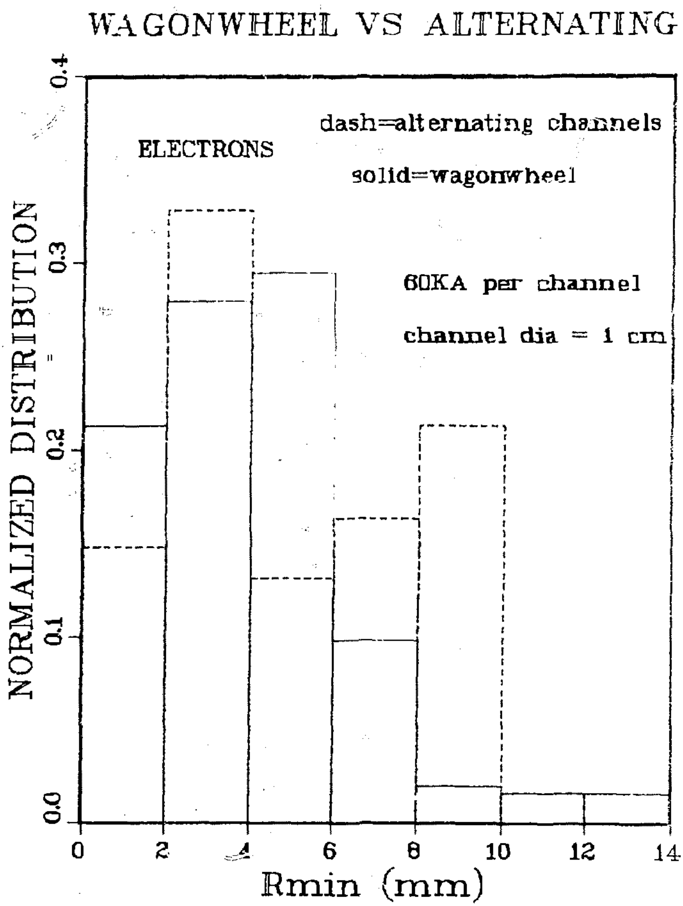
WAGONWHEEL VS ALTERNATING
ELECTRONS
dash=alternating channels
solid=wagonwheel
60KA per channel
channel dia = 1 cm
NORMALIZED DISTRIBUTION
0.0
0.1
0.2
0.3
0.4
0
2
4
6
8
10
12
14
Rmin (mm)

FIGURE 5

disk of N beams converging on a cylindrical surface of radius R_m is

$$G = \frac{1}{4}\, \varepsilon\, N \sin(\pi/N) \approx \frac{1}{4}\, \pi\, \varepsilon \quad (N > 12).$$

The parameter ε is a measure of the effective beam divergence at the end of the channel and is given by

$$\varepsilon \equiv R_o/R_m = r_c/R_m \sin(\pi/N) \;,$$

where r_c is the beam-channel radius, R_o is the geometric overlap radius, and R_m is the mean value of closest approach to the center of the disk as obtained from trajectory calculations using uniform current density plasma channels.

For electrons, the channel current used in the calculations was close to the Alfvén current, so that the beams always came out of the channels hot, and it was found that $\varepsilon_e \approx 4$, independent of the number or size of channels, provided that $R_o > 4\ r_c$. If $R_o < 4\ r_c$ $(N < 12)$, then $R_m \approx r_c$, and $\varepsilon_e \approx \csc(\pi/N)$. Therefore, for a single-disk system of N electron beams the current density gain is

$$G_e = \begin{cases} \pi & N > 12 \\ N/4 & N < 12 \end{cases}$$

The maximum current density gain for multi-disk electron configurations seems to be limited to about 10 (3 disks) from packaging considerations. Future calculations will study multi-disk overlap gain in detail.

Somewhat higher gains are possible for ions. For a given maximum injection angle θ_m of ions at a radial position r_i in a channel of radius r_c $(r_i < r_c)$, the channel current can be picked to just contain the ion beam:

$$I_c \approx \frac{1}{Z_0}\left(\frac{2\,TM}{q}\right)\frac{\sin\theta_m \tan\theta_m}{1-(r_i/r_c)^2} \approx \frac{\theta_m^2}{1-(r_i/r_c)^2} \text{ MAmps (for 2.0-MeV, protons)}$$

where T is the ion energy in MeV, M is the ion mass, and q is the ion's charge state. For example, if $\theta_m = 6.3^\circ$ and $r_i = .75\, r_c$, a current of 50 [illegible] is required for 2.0-MeV protons. The initial effective ion temperature is preserved during the channel transport, so θ_m remains as the important parameter in the overlap estimate.

If the effective ion temperature is large enough that the ion beam can spread more than a channel radius ($R_m \gg r_c$) in the distance R_o, then $R_m \approx R_o \tan\theta_m = r_c \tan\theta_m/\sin(\pi/N)$. Of more interest is the case of high brightness ion beams where $R_o \tan\theta_m < r_c$. The ion beam does not expand much after leaving the channel, and $R_m \approx r_c$. The beam divergence parameter in the gain formula becomes

$$\epsilon_i \approx \begin{cases} \cot\theta_m & (\tan\theta_m > \sin(\pi/N)) \\ f(\theta_m)\csc(\pi/N) & (\tan\theta_m < \sin(\pi/N)) \end{cases}$$

The latter case is the one of principal interest, and $f(\theta_m)$ increases from 1 for $\theta_m \approx \pi/N$ to 2 for $\theta_m \ll \pi/N$. Note that the transition in parameter dependence of ϵ_i occurs at $\theta_m \approx \pi/N$, which is 15° for $N = 12$, and 2° for $N = 90$.

The current density gain factor for ion channel overlap becomes

$$G_i \approx \begin{cases} f(\theta_m)\, N/4 & \text{for } N\theta_m < \pi \\ \pi/4\,\theta_m & \text{for } N\theta_m > \pi \end{cases}$$

Thus, for $N = 12$ and $\theta_m = 2^\circ$, $G_i \approx 6$ (see Fig. 2); and for $N = 90$ with the same divergence angle, $G_i \approx 22$. It should be noted that for thin-shell exploding pusher ion targets, the gain in the energy deposition will be N times that of a single beam and G_i is not a determining factor in the deposited energy.

Again, these single-disk gains can be increased somewhat by using multi-disk arrangements. These simple formulas contain only the crudest estimate of the efficiency of particle transport to the target. Future work will include improved efficiency estimates and modeling.

Some multi-disk calculations for electrons in cylindrical geometry were performed which show effects on electron transport not found in single-disk systems. Five wagonwheel disks were stacked together cylindrically with the combined discharge return currents flowing out along the axis of the system. Eighteen channels per disk gave a total of 90 beams. The superimposed magnetic fields proved to be too large to allow electron transport in all but the central disk which includes the $z = 0$ plane. Since the dominant contribution to P_z near the overlap radius comes from the axial return current channels, this was removed by replacing the axial channels by two conducting sheet disks, one on each end of the stack. Then the superimposed field was non-zero only in the 5 disks between the conducting sheets, and it was due to the beam channel currents alone. However, the calculations showed that electron transport was still cut off in the two outer disks. Conducting sheets were then added between disks to isolate each from its neighbor. Now the net field was due to only those channels in a given disk. The electrons in all disks efficiently propagated to the overlap radius, but the net magnetic field in the overlap region was so low that multiple electron passes through the overlap region seemed unlikely. The electron trajectories for each disk look similar to those shown in Fig. 4.

These multi-disk results may seem to put us on the horns of a dilemma: If we configure the plasma currents to provide large magnetic fields inside the overlap region for efficient electron reflexing, then electrons cannot get to the overlap region. On the other hand, if we configure for good electron transport, the fields in the overlap region are too weak for efficient electron reflexing. However, it seems [illegible] to design configurations which avoid this dilemma by adding other fields in the overlap region as discussed further in Section IV.

III. Thin-Foil Deposition

In this section we introduce collisional effects into the [illegible] plasma-channel transport of Section II in order to study the [illegible] interaction in the presence of the channel fields. We are primarily interested in the beam-target coupling efficiency and the [illegible] deposition. In Section 3.3 we review the results obtained for [illegible] single-disk, multibeam configurations similar to those discussed in Section II, but with cylindrical tantalum foils to [illegible] pusher targets. Before doing so, however, we consider two [illegible] beam-target geometries. First, we investigate axial injection of [illegible] beam into a planar tantalum foil in order to study the [illegible] of beam-foil interaction within channel fields. These results [illegible] potential application to the design of advanced bremsstrahlung [illegible] for effects testing. We then briefly consider injection of a [illegible] converging disk beam between two tantalum foils with axial return [illegible] channels.

3.1. Axial Injection into Single Foil

The initial series of calculations involved the simplest geometrical arrangement: the interaction of a cylindrically symmetric REB with a planar target foil. The magnetic field was assumed [illegible] of an infinitely long plasma channel with a radius of 0.3 cm and a uniform current density of 1.77 x 10^5 amps/cm^2 ($I_c \sim 1.25\ I_A$ for 0.8 MeV). A uniform REB of 0.8-MeV electrons (typical of the Hydra source), having the same initial radius as the plasma channel and a 2π cosine-law angular distribution, was injected into this channel parallel to the channel electron current. An R-Z plot of 21 sample trajectories in the channel field is shown in Fig. 6 where the beam is travelling in the positive-Z direction. Transport over this 1.2-cm distance was roughly 97% efficient due to the Alfvén current limitation, with the radius of the transported beam being slightly larger than the channel radius.

A 12-μm thick tantalum foil with a radius of 1.5 cm was selected as the target. Having verified efficient beam transport in vacuum, we were then justified in injecting the beam at the surface of the target. An R-Z plot of 100 sample trajectories is shown in Figure 7. The front surface of the foil is at Z = 0.0 cm, so that the region Z < 0.0 shows the trajectories of collisionally reflected electrons. Some of the more important quantitative results from this calculation are tabulated in Table I (calculation #1). On the transmission side of the foil there is nothing to prevent continued forward beam propagation so that 98% of the electrons are transmitted, and the mean number of <u>reentries</u> per source electron is only 0.67.

In order to reduce escape by transmission, the channel current on the transmission side of the foil was reversed in calculation #2. The current reversal did inhibit transmission, but as can be seen in the 1000-trajectory R-Z plot of Fig. 8, the electrons simply "walked" out radially until they escaped through the lateral cylindrical escape boundary. The mean number of reentries rose to 3.06, but as is evident

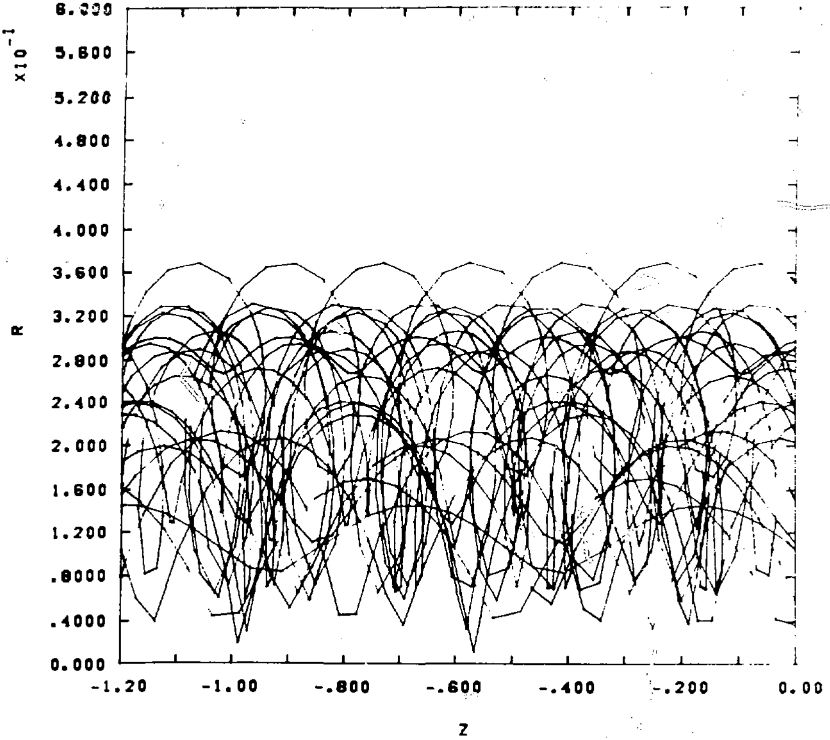
6.000
5.600
5.200
4.800
4.400
4.000
3.600
3.200
2.800
2.400
2.000
1.600
1.200
.8000
.4000
0.000
x10^-1
R
-1.20
-1.00
-.800
-.600
-.400
-.200
0.00
Z

FIGURE 6

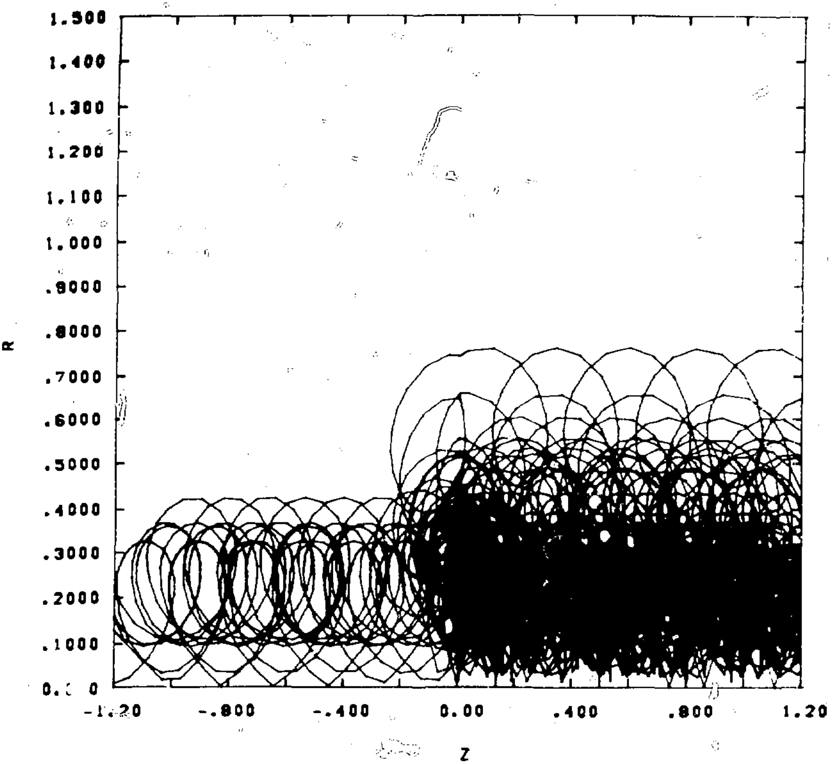
1.500
1.400
1.300
1.200
1.100
1.000
.9000
.8000
.7000
.6000
.5000
.4000
.3000
.2000
.1000
R
-.800
-.400
0.00
.400
.800
1.20
Z

FIGURE 7

TABLE 1

Recapitulation of results obtained for the transport and target-foil interaction of an REB in a plasma-channel magnetic field. Numbers in parentheses are the estimated one-sigma statistical uncertainties expressed as percentages of the given quantities.

Calculation #	Channel Radius (cm)	Approximate Number Escape (%)			Mean Number of Reentries	Beam-Target Coupling Efficiency (%)	Mean Specific Power Deposition (TW/g MA) Within a Radius of	
		Transmission	Reflection	Lateral			1.5 cm	0.3 cm
I-1 [a]	0.3	98	2	1	0.673	8.561 (1)	0.4864 (1)	8.711 (1)
I-2 [b]	0.3	5	2	94	3.064	20.88 (1)	1.187 (1)	7.659 (1)
I-3 [b]	0.5	23	11	[illegible]	5.960	38.90 (1)	2.210 (1)	[illegible] (1)
I-4 [c]	0.5	19	[illegible]	[illegible]	[illegible]	54.15 (1)	3.077 (1)	9.51 (1)
I-5 [d]	0.5	69	[illegible]	[illegible]	[illegible]	[illegible] (2)	[illegible] (2)	11.8[illegible] (1)

[a]Conduction electron current density of ~ 180 kA/cm^2 in the REB direction on both sides of foil.

[b]Conduction electron current density of ~ 180 kA/cm^2 in the same and opposite directions as the REB on the injection and transmission sides of the foil, respectively.

[c]Conduction electron current densities of ~ 180 kA/cm^2 and ~ 380 kA/cm^2 in the same and opposite directions as the REB on the injection and transmission sides of the foil, respectively.

[d]Conduction electron current densities of ~ 180 kA/cm^2 and ~ 380 kA/cm^2 in the same direction as the REB on the injection and transmission sides of the foil, respectively.

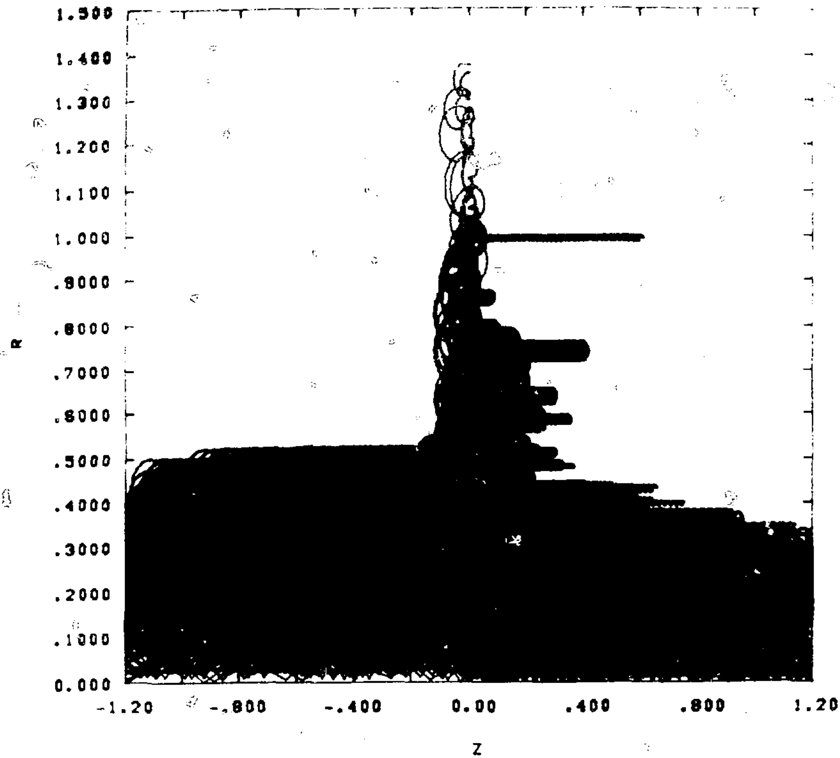
1.500
1.400
1.300
1.200
1.100
1.000
.9000
.8000
.7000
.6000
.5000
.4000
.3000
.2000
.1000
0.000
R
-1.20
-.800
-.400
0.00
.400
.800
1.20
Z

lost through transmission escape. However, even though there was a substantial drop in the total energy deposited, the amount of energy deposited within the initial beam radius was the highest achieved in this single-foil series. Furthermore, the mean number of reentries is more than 4.5 times that obtained in calculation #1--the only other case where the field on the transmission side was in the direction of beam propagation.

The results of these single-foil calculations can be understood by consideration of the classes of electron orbits in a uniform current density channel. Figure 10 presents a qualitative schematic representation of a plasma channel for the following discussion. The radius of the current-carrying channel is r_c and the radius which encloses the Alfvén critical current for the energy of the beam electrons is r_A. An electron moving axially feels a Lorentz force which is radially inward (F_+) if it is moving in the same direction (v_+) as the plasma conduction electrons. If its axial velocity is anti-parallel (v_-) to the electron conduction flow, the Lorentz force is radially outward, or defocusing. To lowest order, then, electrons injected with v_+ tend to be confined in the channel, whereas electrons with v_- tend to be ejected from the channel. This is true for electrons injected inside r_A, which is labeled the non-adiabatic region. Since the scale length of the magnetic field is smaller than the Larmor radius in this region, electrons do not complete a Larmor orbit and adiabatic drift theory does not apply.

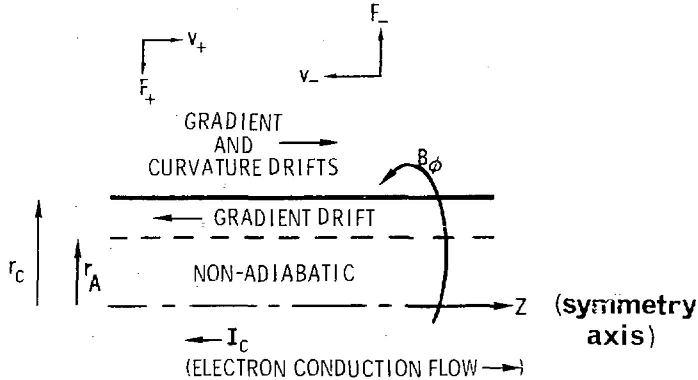

V_+
F_+
F_-
V_-
GRADIENT AND CURVATURE DRIFTS
B_ϕ
GRADIENT DRIFT
r_C
r_A
NON-ADIABATIC
Z
(symmetry axis)
I_C
(ELECTRON CONDUCTION FLOW)

FIGURE 10

For electron orbits outside r_A, the field is strong enough to bend the electron trajectories into complete Larmor orbits, so adiabatic drift theory does apply. The two drifts of importance for axial transport are the grad-B drift and curvature drift. The latter provides guiding-center motion in the same direction as the electron conduction current. The direction of the gradient drift depends on whether the field is increasing or decreasing with radius. The gradient drift inside r_c is opposed to the direction of the electron conduction flow, and it is in the same direction for orbits outside the channel radius. The ratio of the gradient drift to the curvature drift is given by the kinetic energy ratio $w_\perp/w_\parallel$, where $w_\parallel$ is the electron kinetic energy along the magnetic field (azimuthal) direction. Trajectory calculations have been performed where this ratio was computed and the gradient drift was found to be predominant.

Based on these considerations, the single-foil results can be explained as follows. In calculation #1, the electrons lost very little energy in a single pass. Since most of them were in the non-adiabatic propagation region, the foil interaction represented a small perturbation in their trajectories and they just continued propagating along the channel on the transmission side. In calculation #2, the current on the transmission side was reversed, so that every time an electron passed through the foil it found itself in a defocusing field, resulting in a succession of radially outward steps and a predominantly lateral escape. Calculations #1 and #2 had $r_A \approx r_c$ for injected electrons so that the annular region of predominantly backward gradient drift shown in Fig. 10 did not exist. The small fraction of escape by reflection was probably due to sufficient energy loss in foil transits by some electrons so that they became adiabatic inside r_c and could gradient drift away from the foil. Calculation #3 supports this because in this case $r_A < r_c$ for the initial electron energy and the backward gradient-drift region must be crossed by laterally escaping electrons, resulting in larger transmission and reflection escape by this mechanism. By increasing the field on the transmission side in calculation #4, the predominant effect was that the radial step was made much smaller on the transmission side, causing more reflexing through the foil, higher deposition and lower escape fractions. The fact that the fields on both sides of the foil were defocusing for reflexing electrons in calculations 2-4 prevented significant enhanced energy deposition inside the initial beam radius. In calculation #5, the current on the transmission side was reversed, so that on this side the reflexing electrons took an inward radial step resulting in the best specific deposition obtained in the single foil calculations. The relatively large transmission coefficient was due to three effects:

a) transmission of the central core of the incident electron beam inside the radius of the Alfvén current on the transmission side,

b) grad-B drift of electrons outside the channel radius on the transmission, and

c) curvature drift of those electrons that exit the transmission side of the foil with velocities nearly parallel to the magnetic field.

It has become obvious to us that the deposition attainable in these calculations was limited by the existence of axial particle drifts away from the foil. This has led us to propose different magnetic field configurations in Sec. IV on the transmission side of the foil so that any particle drifts will be beneficial.

3.2 Radial Injection Between Foils

Another scheme investigated was that of radial injection of a disk beam between two foils. Having already verified propagation of the REB's through the plasma channels (Fig. 6) and assuming that they combine to form a disk beam at the overlap radius, we attempted to simulate this scheme with a 0.6-cm long, 1.0-cm radius, uniform cylindrical source between two parallel, 1.0-cm radius, 12-μm thick planar foils. For the source-electron directions we assumed a cosine-law distribution with respect to the inward normal to the cylinder over a 2π solid angle. The region between the foils was taken to be field-free. Outside the foils the field was assumed to be that of a uniform return current of 150 kA (one half the estimated 300 kA total channel current) with a radius of 1.0 cm and with conduction electron flow directed away from the foils. Results from this first calculation (#1) are shown in Table II. An R-Z plot of 100 sample trajectories is shown in Fig. 11.

In calculation #2 of Table II, the channel return currents were assumed to flow in a solid conductor with a radius of 0.025 cm. There is some modest improvement over calculation #1 with a 50 percent increase in the energy deposition within 0.3 cm of the axis.

In calculation #3, the return currents of the previous calculation were simply reversed (toward the foils). This rather unrealistic scheme merely led to 100 percent lateral escape as shown in Fig. 12, with little improvement in the parameters of Table II.

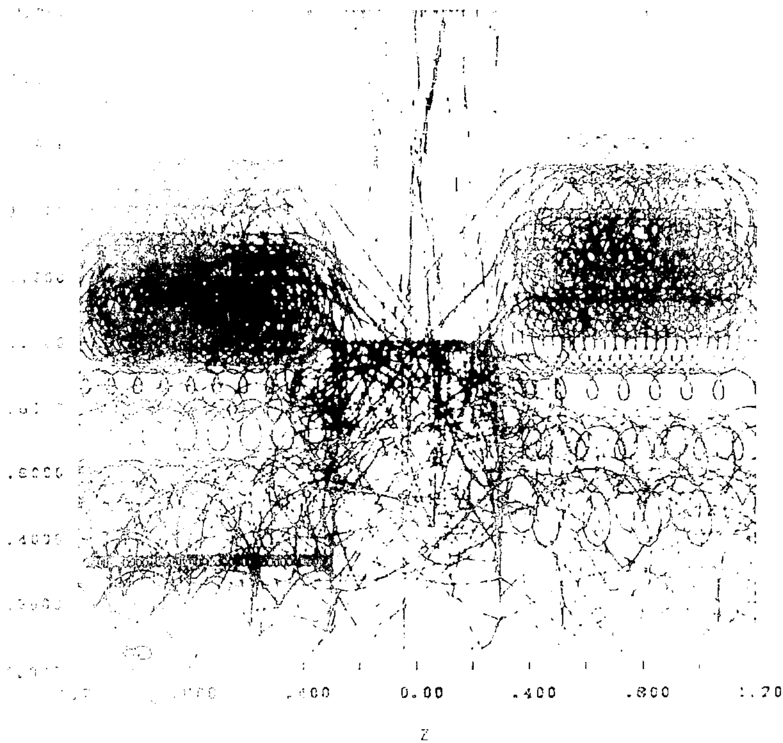
.8000
.4000
.400
0.00
.400
.800
1.20
Z

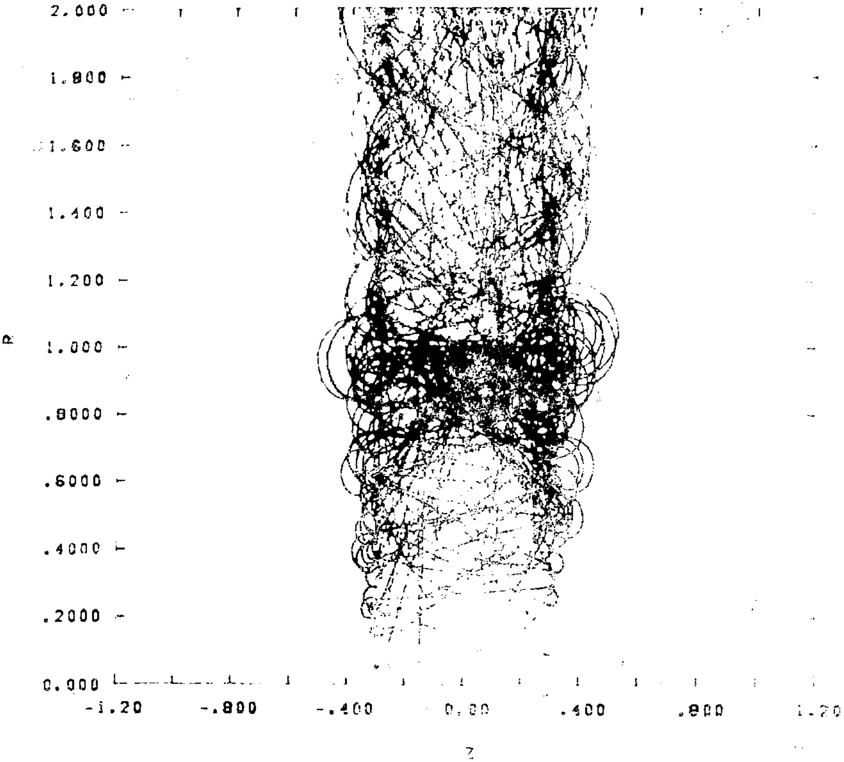
2.000
1.800
1.600
1.400
1.200
1.000
.8000
.6000
.4000
.2000
0.000
R
-1.20
-.800
-.400
0.00
.400
.800
1.20
Z

TABLE II

Recapitulation of results obtained from the CYLEM model of the transport and interaction of an REB with a double-foil target in a plasma channel magnetic field. Numbers in parentheses are the estimated one-sigma statistical uncertainties expressed as percents of the given quantities.

Calculation #	Approximate Number Escape (%) Transmission	Reflection	Lateral	Mean Number of Entries	Beam-Target Coupling Efficiency (%)	Average Specific Power Deposition (TW/g/MA) Within a Radius of 1.0 cm	0.3 cm
1	35	36	31	1.743	9.229 (1)	0.5899 (1)	0.5976 (3)
2	35	33	33	2.267	12.21 (1)	0.7805 (1)	0.9094 (3)
3	0	0	101	1.937	10.17 (1)	0.6502 (1)	0.5338 (3)

3.3 Multiple REB Transport in Nonaxisymmetric Plasma-Channel Fields Proto-II

The magnetic fields for the standard wagonwheel configuration discussed in Sect. II were incorporated into the CYLEM code. Since the standard cosine distribution used for beam injection results in some beam trajectories outside the channel as shown in Fig. 6, we decided to modify the distribution to produce a beam radius matched to the channel radius. We employed a modified cosine-law distribution in which the cylindrical coordinate components of the initial velocities are defined by

$$V_r' = V_r[1 - (r/r_c)^2]^{1/2}$$

$$V_\phi' = V_\phi$$

$$V_z' = V_z[1 + (V_r/V_z)^2 (r/r_c)^2]^{1/2} ,$$

where the unprimed components are sampled from the cosine-law distribution, r is the radial source coordinate, and r_c is the radius of the plasma channel. This modification results in a vanishing radial component at $r = r_c$ and an unmodified cosine-law at r = 0.0. With this distribution we obtain the trajectory plot shown in Fig. 13. The REB has a well-defined envelope with a beam radius very nearly equal to the channel radius.

We are now in a position to discuss the predictions of the CYLEM code for the interaction of multiple REB's from Proto-II with can-shaped tantalum targets having dimensions of the order of the channel radii. The bulk of the calculations involves a single disk of twelve 60 kA plasma channels (like spokes in a wheel) injecting the twelve REB's

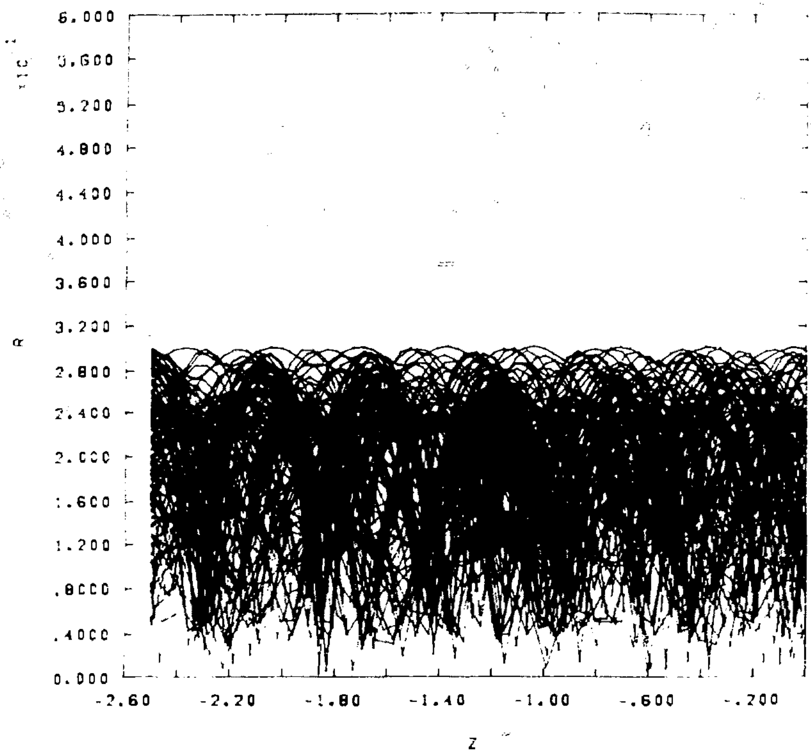

6.000
5.600
5.200
4.800
4.400
4.000
3.600
3.200
2.800
2.400
2.000
1.600
1.200
.8000
.4000
0.000
α
-2.60
-2.20
-1.80
-1.40
-1.00
-.600
-.200
Z

radially through the cylindrical surface of the can. Electrons are sampled uniformly over the plasma channel cross section at a distance of 2.0 cm from the Z axis. Half the total channel current was returned axially through each of the plasma channels at either end of the can. Our primary concern was the dependence of REB-target coupling efficiency and specific power deposition upon dimensional parameters of the target and plasma channels. We also tallied the mean number of target entries per source electron. In contrast to the mean number of reentries tallied in Sec. 3.1, this talley includes the initial entry of the source electrons.

Results of the fifteen calculations are summarized in Table III. Except where footnotes indicate otherwise, beam channel radii were 0.3 cm, radii of return current channels were 1.0 cm, and the magnetic field was assumed to be zero inside the can. From calculations #1 through #4, it appears that a wall thickness of about 30 μm is best for optimizing both coupling efficiency and specific power deposition. Calculations #2 and #3 show that the presence of the field within the can has little effect. Calculations #6, #8, and #14 show that reducing the can radius increases specific power deposition, but reduces the beam-target coupling efficiency. In calculation #5, an attempt to prevent escape of beam electrons by placing total stopping "reflectors" opposite each end of the can failed because the drift due to the return current channel fields prevented transport back to the target. Most reductions in dimensional parameters had only a modest effect on the results. However, the final calculation shows that specific power deposition is approximately

TABLE III

Recapitulation of results obtained from the CY[illegible] model of multiple [illegible] transport in nonaxisymmetric plasma channel fields fo[illegible]roto-II. Numbers in parentheses after coupling efficiencies are the estimated one-sigma statistical uncertainties expressed as percentages of the given quantities.

Calculation #	Can Radius (cm)	Can Length (cm)	Wall Thickness (μm)	Can Mass (g)	Mean Number of Entries	Beam Target Coupling Efficiency (%)	Specific Power Deposition (TW/g/MA)
1[a]	1.2	0.4	12	0.2403	5.838	16.27 (2)	1.016 (2)
2[a]	1.2	0.4	30	0.6008	5.607	40.28 (3)	1.006 (3)
3	1.2	0.4	30	0.6008	5.904	42.80 (2)	1.069 (2)
4	1.2	0.4	60	1.2015	4.475	61.87 (1)	0.772 (1)
5[b]	1.2	0.4	30	0.6008	-----	41.55 (2)	1.037 (2)
6	0.8	0.4	30	0.3004	3.659	25.46 (2)	1.271 (2)
7	1.2	0.6	30	0.6759	6.300	45.05 (2)	1.000 (2)
8	0.8	0.6	30	0.3505	4.273	30.18 (3)	1.292 (3)
9	1.2	0.6	40	0.9012	5.901	56.34 (2)	0.938 (2)
10[c]	1.2	0.6	30	0.6759	6.419	45.76 (2)	1.016 (2)
11[a,c]	1.2	0.6	30	0.6759	6.218	44.79 (3)	.994 (3)
12[c,d]	1.2	0.6	30	0.6759	6.858	49.03 (3)	1.088 (3)
13[a,c,d]	1.2	0.6	30	0.6759	6.571	45.65 (2)	1.013 (2)
14[c,d]	0.8	0.6	30	0.3505	4.868	33.74 (3)	1.[illegible]44 (3)
15[c,d,e]	0.6	0.3	30	0.1690	6.120	43.80 (4)	3.888 (4)

[a] Field on inside can.

[b] 0.4-cm tantalum reflectors opposite each end of can.

[c] Axial decay length of magnetic field reduced to 0.3 cm.

[d] Radius of return current plasma channel reduced to 0.3 cm.

[e] Radius of beam current plasma channel reduced to 0.15 cm.

proportional to the inverse square of the beam channel radius w

other dimensions are scaled accordingly, with little or no loss

target coupling efficiencies. Figure 14, where trajectories i

can are not shown, was obtained for calculation #. It is typi

trajectory plots for the calculations listed in Table III.

We also carried out a series of calculations in which, sta

from calculation #7, we successively increased the plasma re

by factors of two. There was no noticeable increase in eithe

target coupling efficiency or in the specific power depositio

appears that the effect of the decreasing Larmor r , which

have increased stagnation, was offset by an increa

caused by the increasing magnetic field of the ret cu

Again, in this series of calculations, we hav

limited by unfavorable particle drifts away from t

the next section we propose some configurations w

from these effects.

IV. Summary

One of the most important things learned in

role of particle drifts in systems with axial c

electrons provided the principal escape mecha

beams must be transported in current-carrying

little that can be done to change the field c

side of the target foil. However, the fiel

transmission side of the foil can be ch

drifts and prevent beam propagation

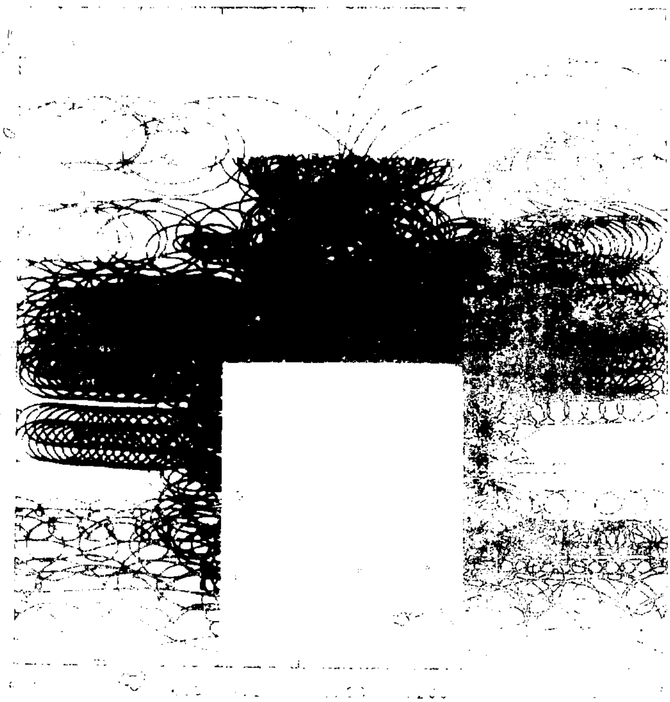

is a single-ended cusp which produces azimuthal steps for reflexing electrons on the transmission side, and a mirror point to minimize beam transmission. The gradient drifts are also azimuthal, so the beam does not spread on the transmission side of the foil. Calculations with this type of single-beam geometry are planned.

It was found that multi-disk systems must be magnetically isolated from each other to allow efficient beam transport to the overlap region. This results in a nearly field-free overlap region if the channel currents are returned along the conducting sheets between disks. Although it is not necessary to return the channel currents in this way, it is desirable to avoid large azimuthal magnetic fields in the overlap region because of the undesirable gradient drifts they cause. A better field configuration in the overlap region may be an axial field with mirror points just outside the axial extent of the overlap region. Such a field could be applied by a small axial Helmholtz-coil arrangement. The mirrors would prevent axial electron loss and the axial field results in azimuthal steps and azimuthal gradient drifts inside the target foil. Some beam loss would still occur on the channel side of the target foil. Studies with this configuration are also planned.

Analytical estimates of overlap current density gain for electrons and ions have been derived for cylindrical target surfaces in single wagonwheel disk configurations. Calculations have produced overlap gains of up to 3 for a single disk of electrons and up to 6 for protons. These studies will be continued to spherical configurations.

References

1. J. A. Halbleib, Sr. and W. H. Vandevender, J. Appl. Phys. 48, 2312 (1977).

2. M. A. Sweeney and A. V. Farnsworth, Jr., to be published.

3. T. P. Wright, J. Appl. Phys. 49 (7), 3842 (1978).

4. P. A. Miller, R. I. Butler, M. Cowan, J. R. Freeman, J. W. Poukey, T. P. Wright, and G. Yonas, Phys. Rev. Lett. 39, 92 (1977).

Distribution:

Jon Farber
Defense Nuclear Agency
Washington, DC 20305

Dr. Sheldon Kahalas
Plasma Program Manager
Division of Laser Fusion
U. S. Energy Research and
Development Administration
Washington, DC 20545

Dr. Allen Kolb
Maxwell Laboratories, Inc.
9244 Balboa Ave.
San Diego, CA 92123

Dr. Sidney Putnam
Physics International
2700 Merced St.
San Leandro, CA 94577

Dr. Norman Rostoker
University of California
Department of Physics
Irvine, CA 92664

Dr. L. I. Rudakov
I. V. Kurchatov Institute of Atomic Energy
Moscow
USSR

4000	A. Narath		
	Attn:	4300	R. L. Peurifoy
		4400	A. W. Snyder
		4500	E. H. Beckner
		4700	J. H. Scott
4200	G. Yonas		
4210	J. B. Gerardo		
4230	M. Cowan		
4231	J. H. Renken		
4231	J. A. Halbleib (5)		
4231	J. E. Morel		
4232	W. Beezhold		
4234	R. E. Palmer		
4240	G. W. Kuswa		
4241	J. R. Freeman (7)		
4241	T. P. Wright (15)		
4242	L. P. Mix (7)		
4244	P. A. Miller (6)		
4247	M. M. Widner (8)		
4250	T. H. Martin		
4251	G. W. Barr		
4252	J. P. VanDevender (4)		
4253	K. R. Prestwich (7)		
4254	S. A. Goldstein		
8266	E. A. Aas (2)		
3151	W. L. Garner (3) for DOE/TIC Public Release		
3144	Central Tech. Files (4)		
3172-3	R. P. Campbell (25) For DOE/TIC		